Supporting Information for

Interfacial electron transfer in heterojunction nanofibers for highly efficient oxygen evolution reaction

Lei Fu,[a] Jun Zhou,*[a] Qinyuan Deng,[a] Jiaming Yang,[a] Qinghao Li,[a] Zihe Zhu,[a] and Kai Wu[a]

[a]*Center of Nanomaterials for Renewable Energy, State Key Laboratory of Electrical Insulation and Power Equipment, Xi'an Jiaotong University, Xi'an 710049, People's Republic of China*

*Email: zhoujun@mail.xjtu.edu.cn

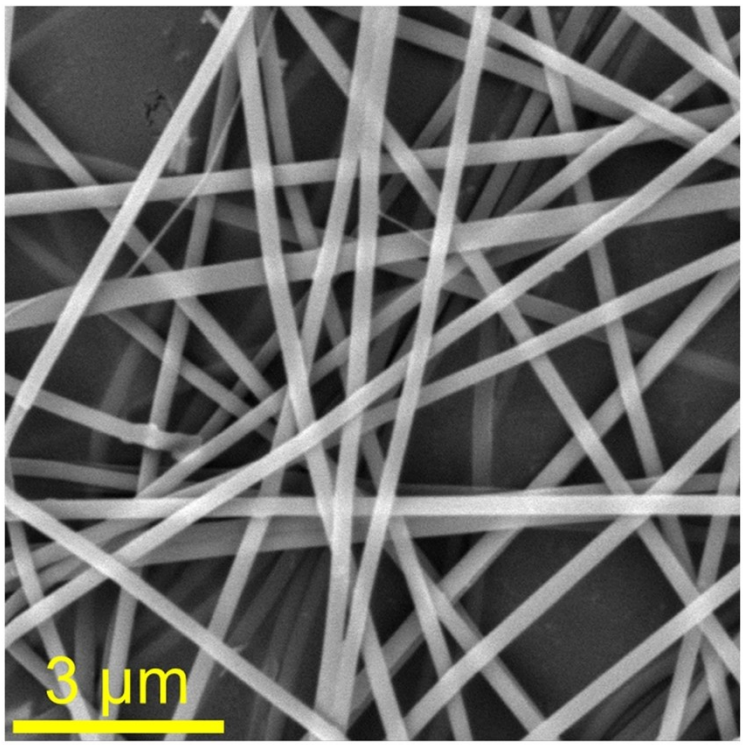

Figure S1. SEM image of precursor SCF nanofibers synthesized by the electrospinning method before calcination.

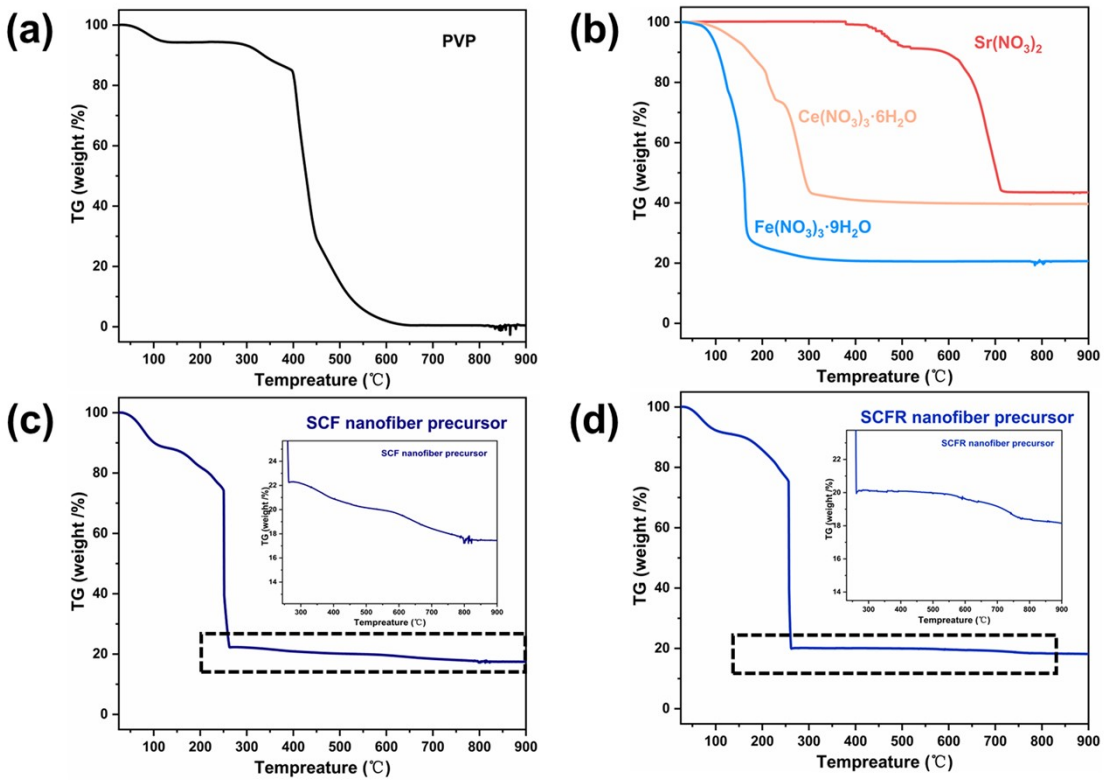

Figure S2. TGA analysis of (a) PVP, (b) $Sr(NO_3)_2$, $Ce(NO_3)_3 \cdot 6H_2O$, and $Fe(NO_3)_3 \cdot 9H_2O$, (c) SCF nanofiber precursor, and (d) SCFR nanofiber precursor. Data were collected under air atmosphere using a temperature ramp rate of 10 °C min^{-1}.

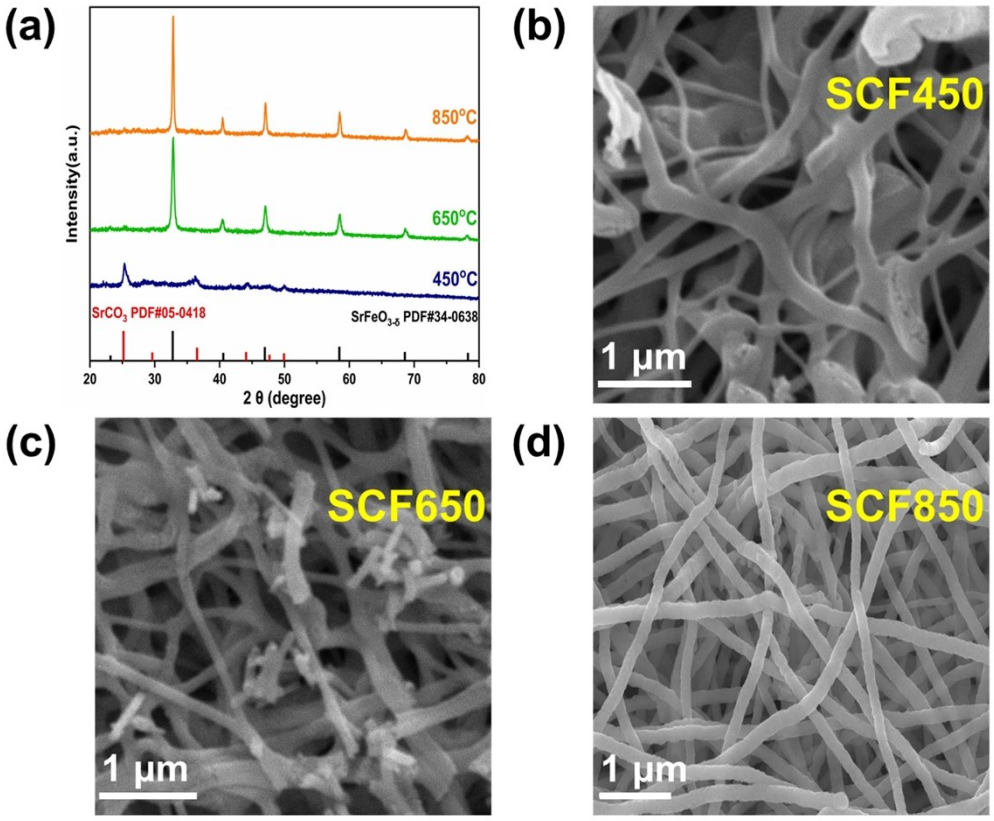

Figure S3. (a) XRD patterns of SCF nanofiber at different calcination temperatures. (b-d) SEM images of SCF nanofibers at different calcination temperatures of (b) 450 ℃, (c) 650 ℃, and (d) 850 ℃.

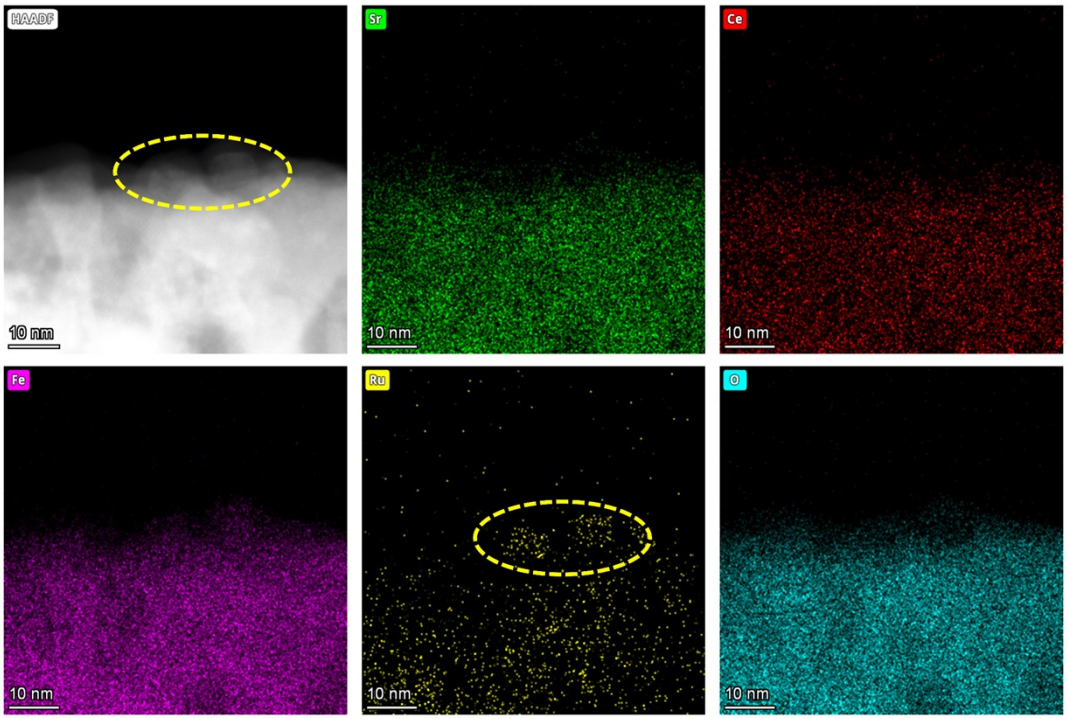

Figure S4. HAADF image and EDS mapping of SCFR-Ru nanofibers, confirming the exsolution of Ru nanoparticles.

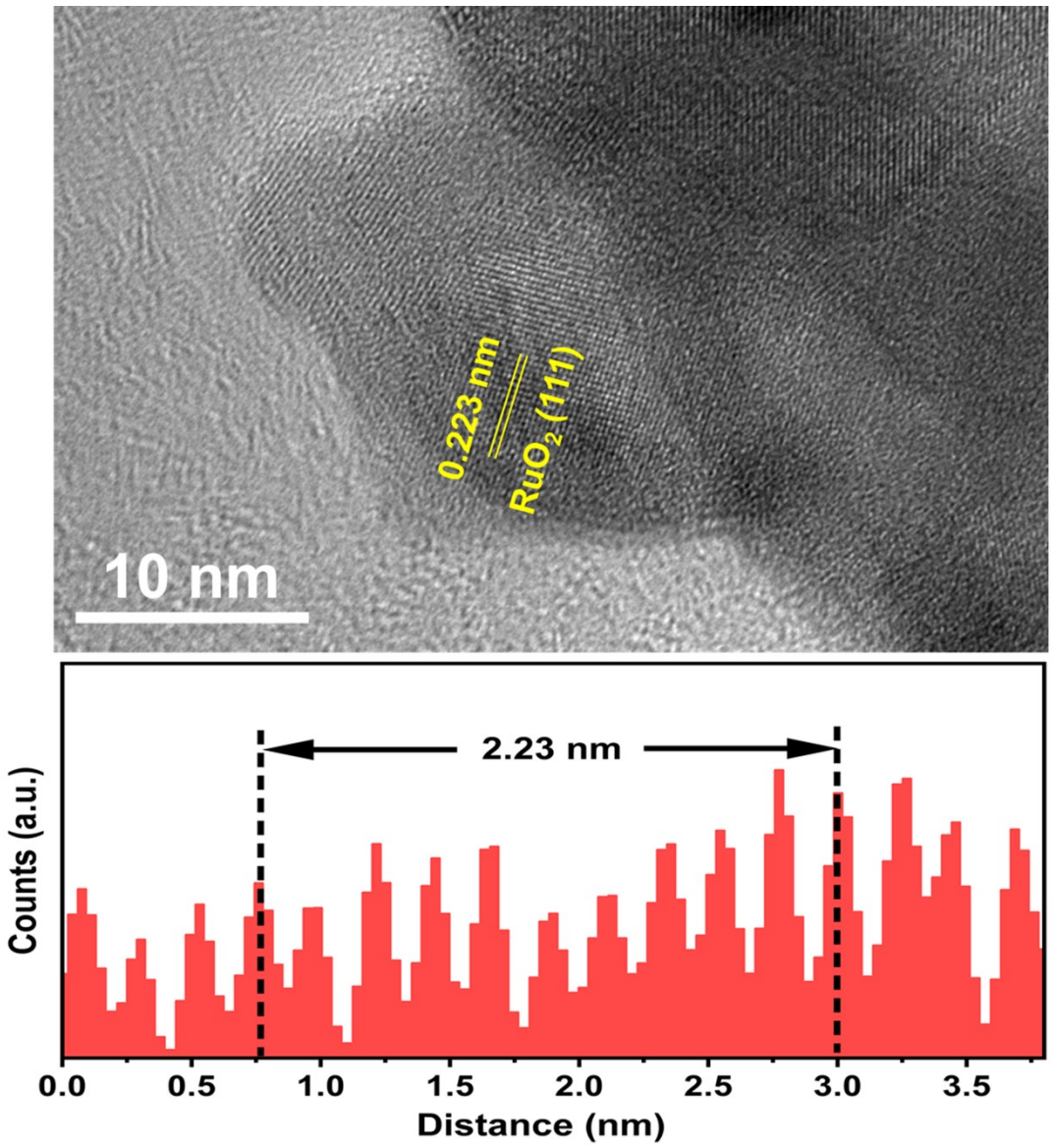

Figure S5. HAADF image and corresponding intensity profile of SCFR-RuO_2.

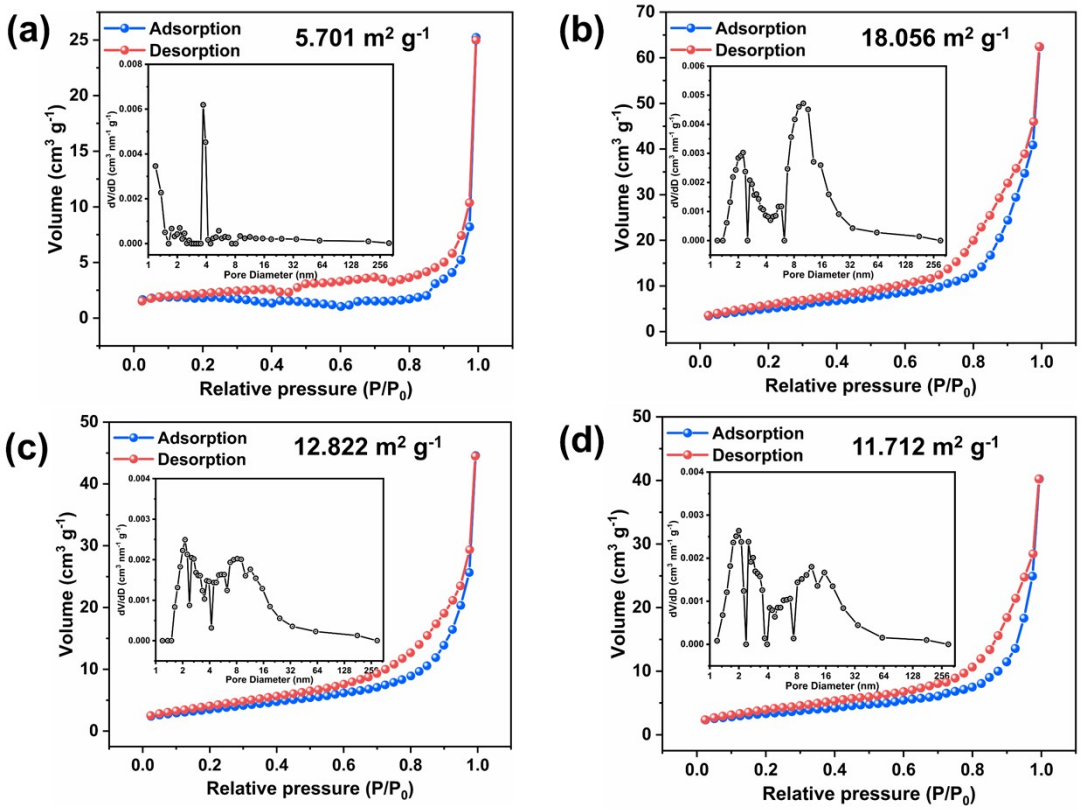

Figure S6. Nitrogen adsorption/desorption isotherms of (a) SCF, (b) SCFR, (c) SCFR-Ru and (d) SCFR-RuO_2. Insets are the corresponding pore size distribution curves.

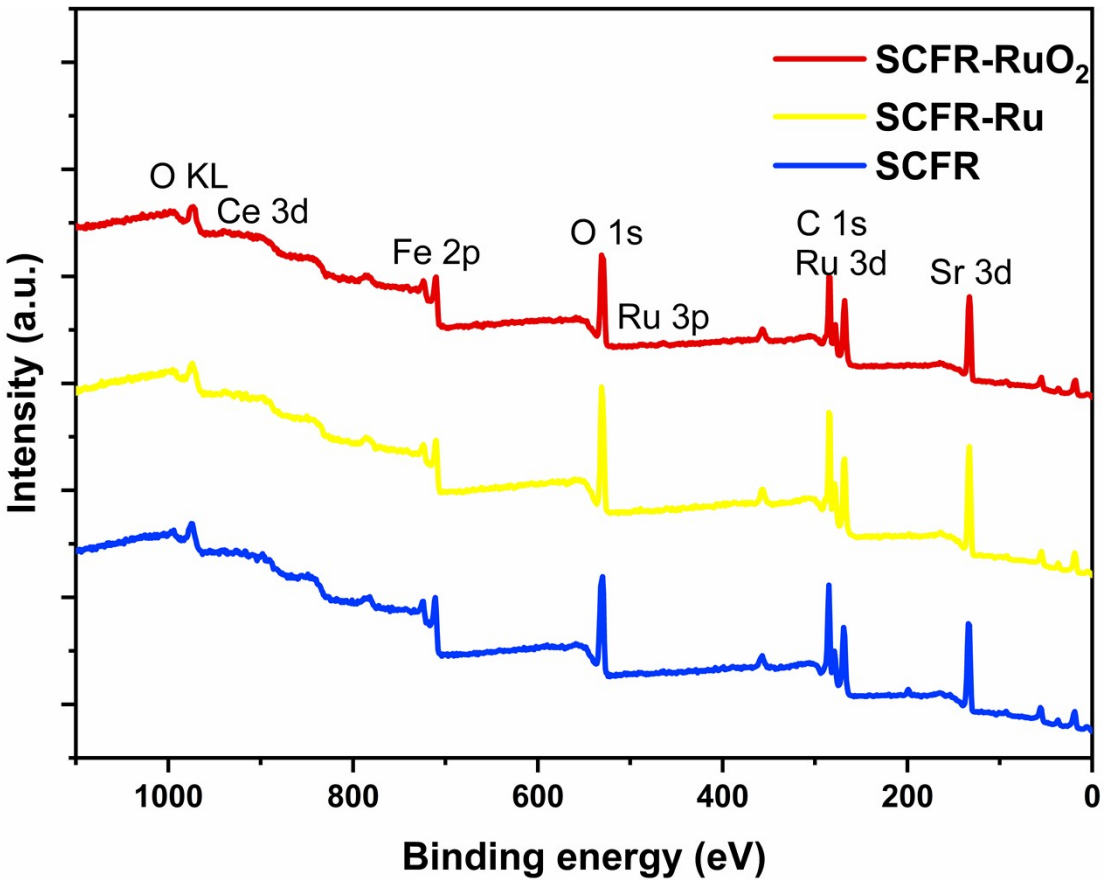

Figure S7. XPS survey spectra of SCFR, SCFR-Ru and SCFR-RuO_2.

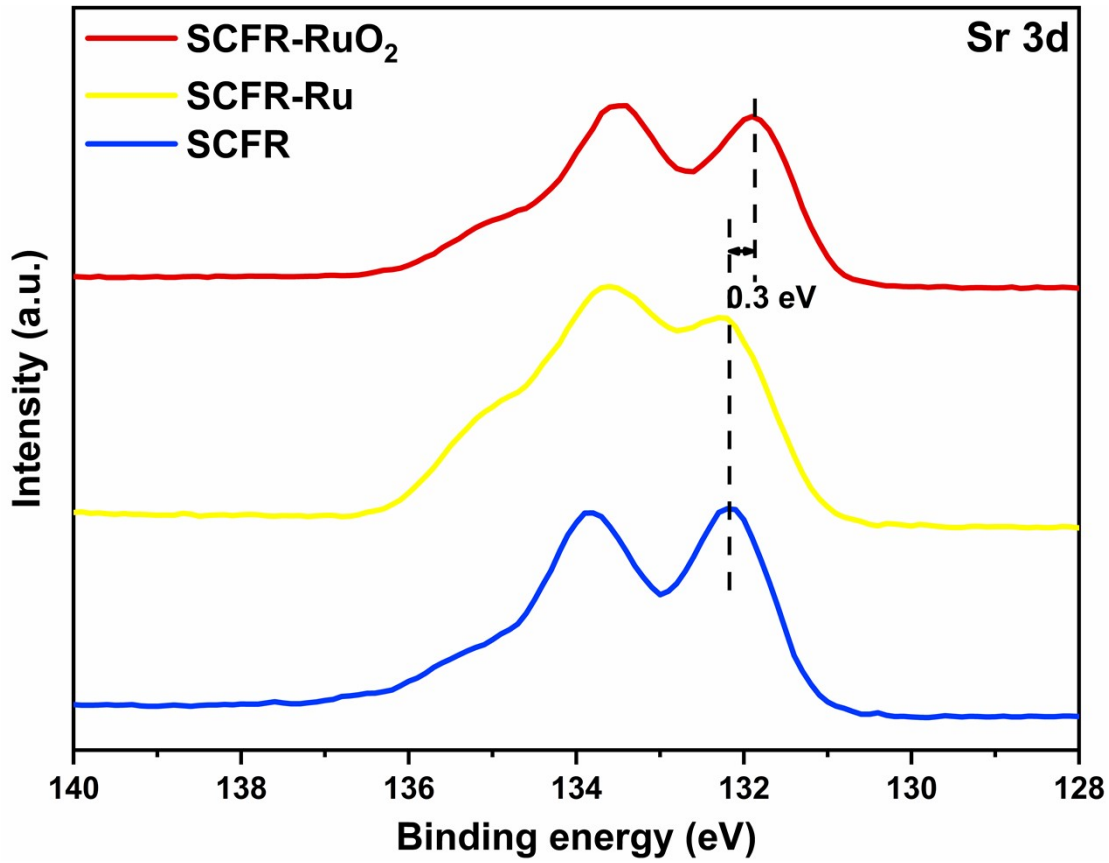

Figure S8. Sr 3d spectra of SCFR, SCFR-Ru and SCFR-RuO_2.

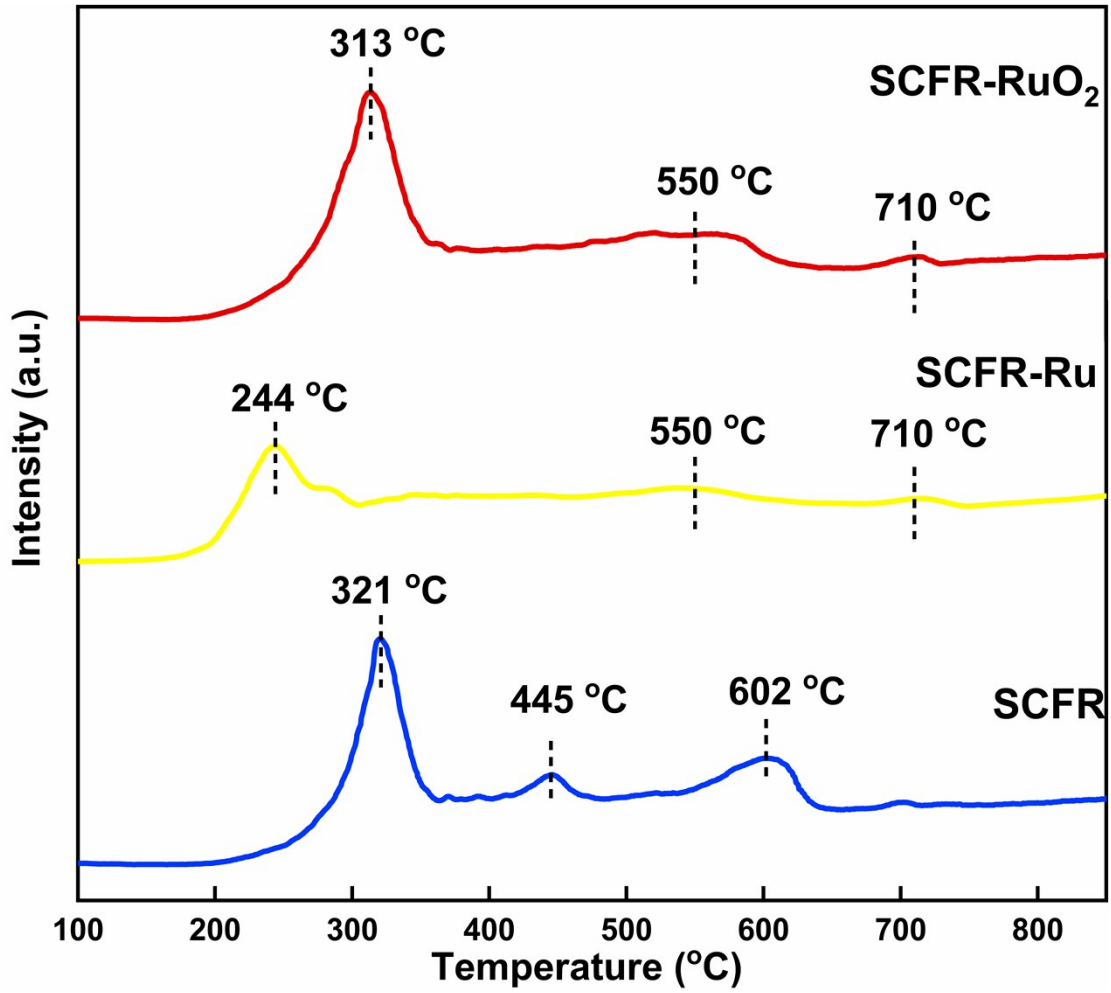

Figure S9. H_2-TPR spectra of SCFR,SCFR-Ru, and SCFR-RuO_2.

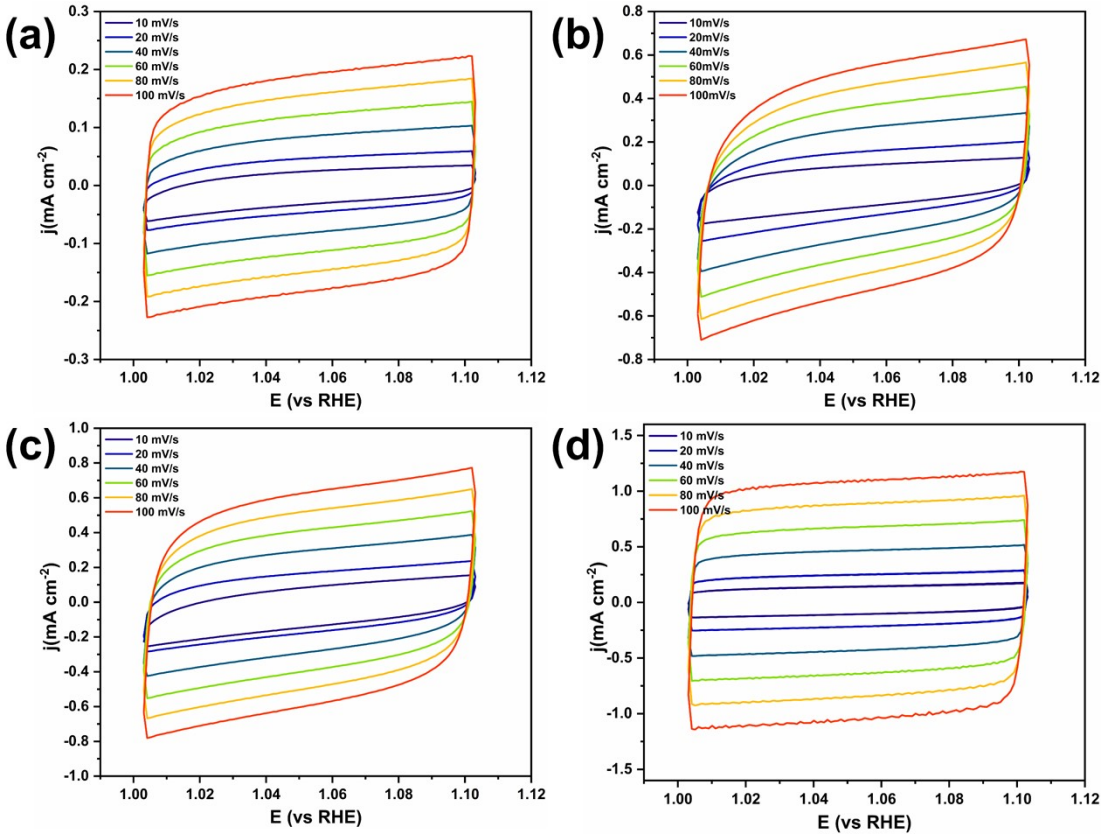

Figure S10. CV curves at different scan rates of (a) SCF, (b) SCFR, (c) SCFR-Ru, and (d) SCFR-RuO_2.

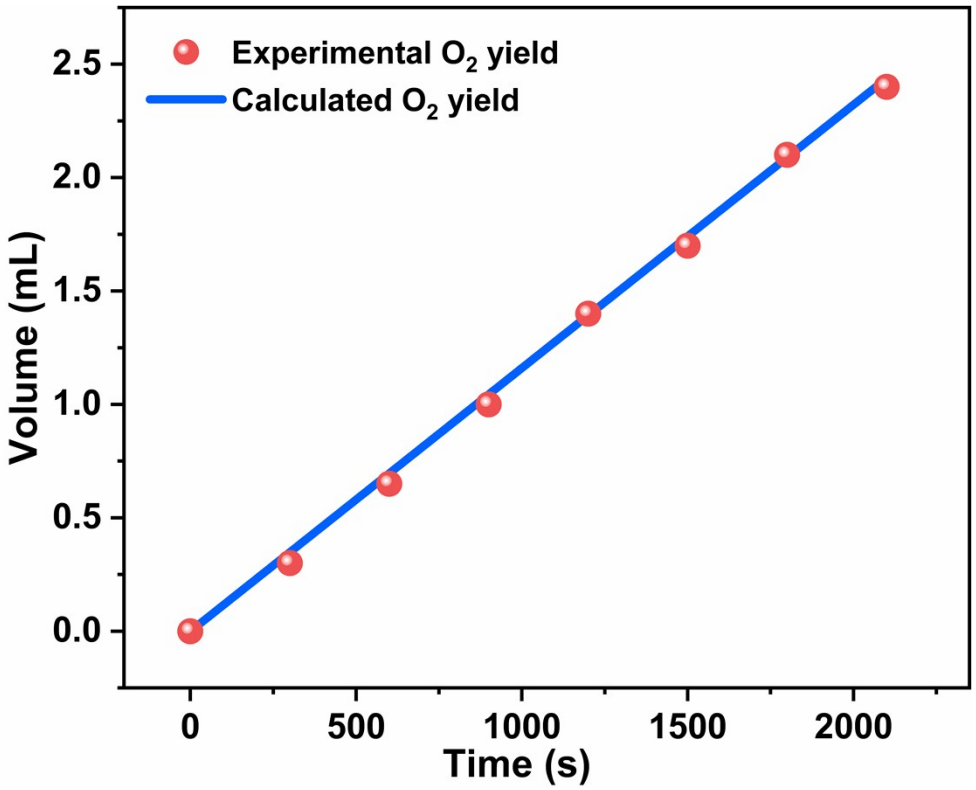

Figure S11. Faradic efficiency of SCFR-RuO_2 for OER at a constant current density of 80 mA cm^{-2}.

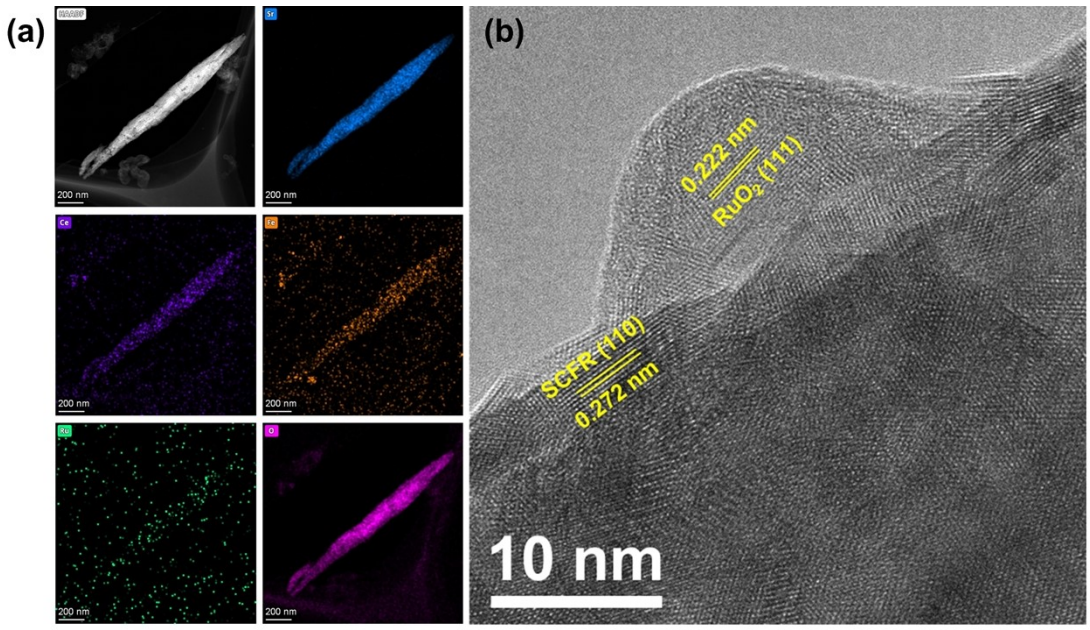

Figure S12. (a) EDS mapping and HRTEM image (b) of SCFR-RuO_2 nanofibers after stability test.

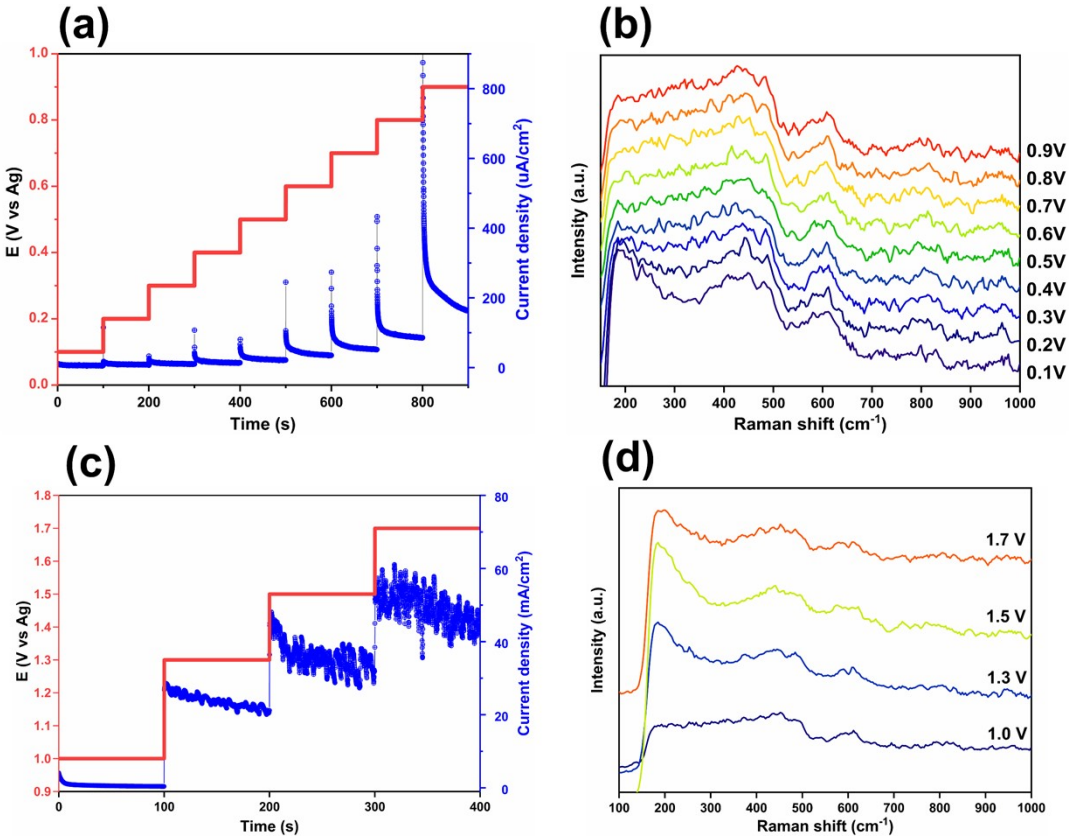

Figure S13. *In-situ* Raman characterizations. (a, c) Multipulsed amperometric curves of SCFR-RuO_2 under different potential of (a) 0.1 V – 0.9 V and (b) 1.0 V – 1.7 V. (b, d) In-situ Raman shift of SCFR- RuO_2 under different potential of (b) 0.1 V – 0.9 V and (d) 1.0 V – 1.7 V.

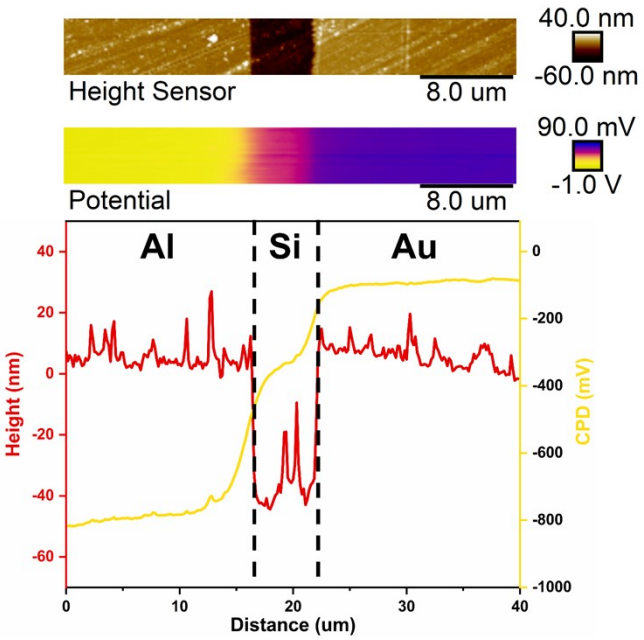

Figure S14. Topography and Potential images and corresponding profiles of Al-Si-Au sample.

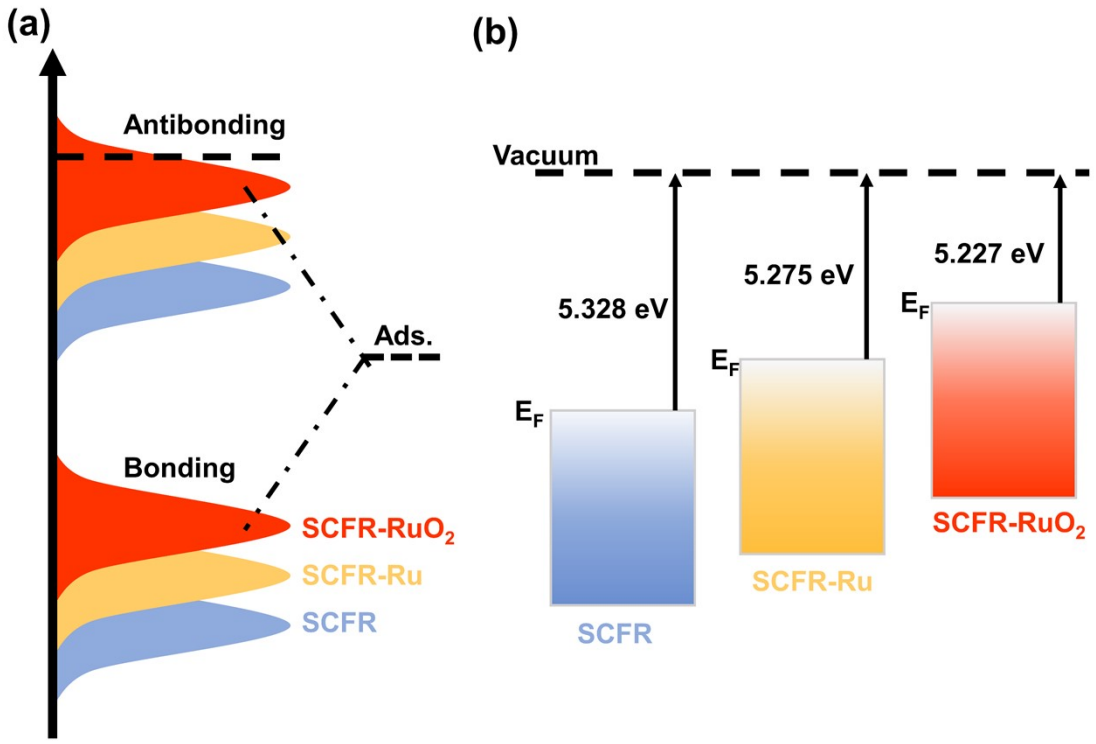

Figure S15. Schematic illustration of (a) bond formation between the catalyst surface and the adsorbates (Ads.), and (b) work functions.

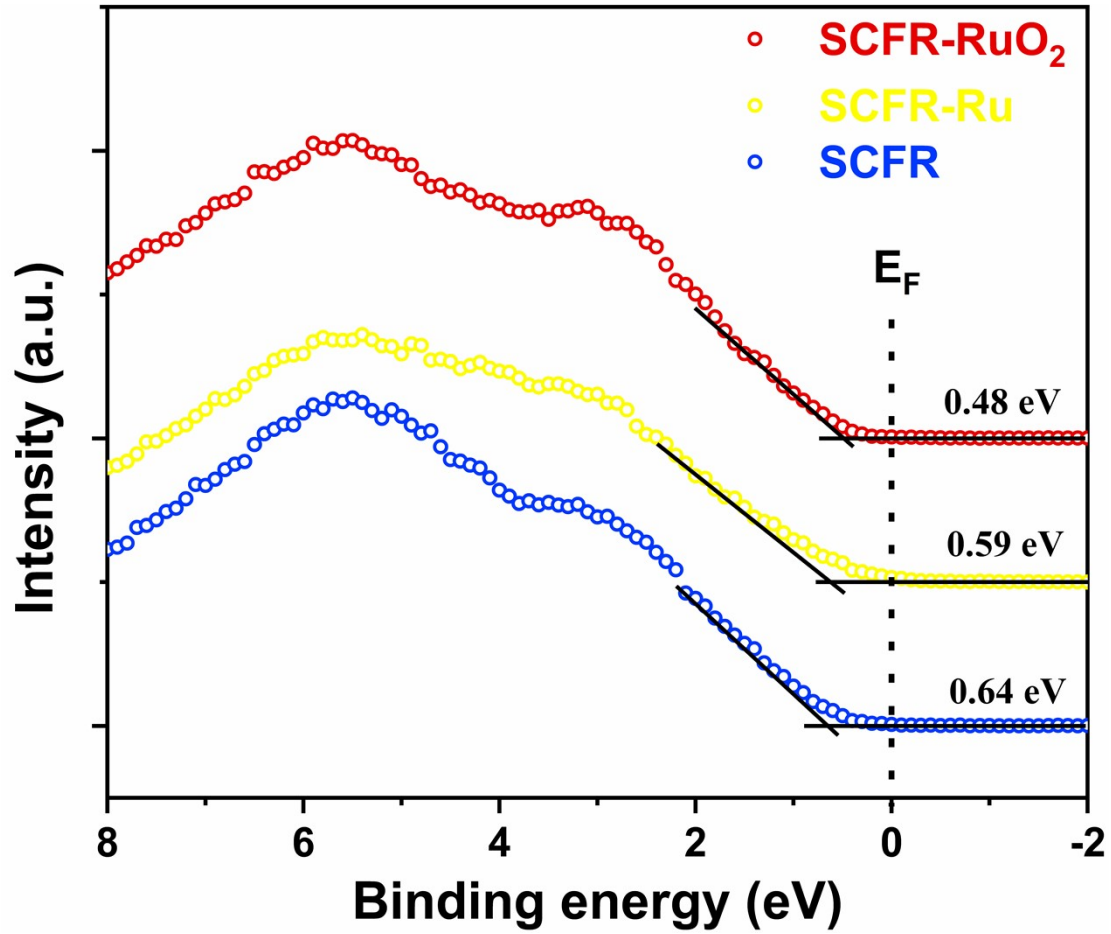

Figure S16. Enlarged view of the VB spectra of SCFR, SCFR-Ru, and SCFR-RuO_2, showing a gradual shift of the VB maximum (VBM) towards the Fermi level (E_F). The VBM is determined by linear extrapolation of the leading edge of the VBM to zero baseline intensity.

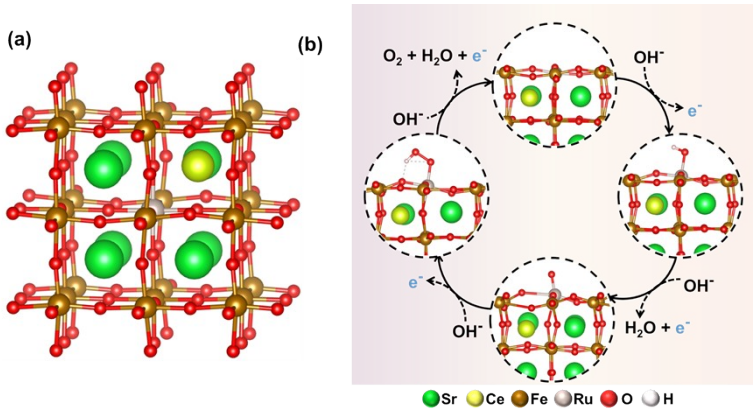

Figure S17. (a) Theoretical model of bulk $Sr_7Ce_1Fe_7Ru_1O_{24}$. (b) Proposed four-electron mechanism diagram toward OER in the absence of RuO_2.

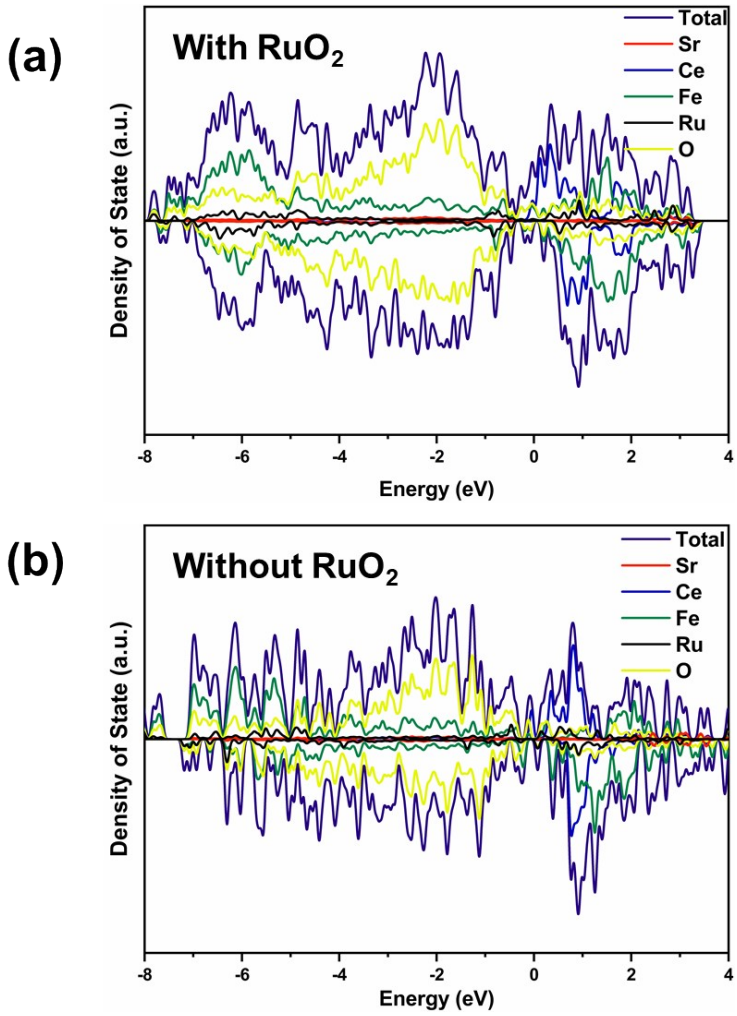

Figure S18. Calculated DOS plots in presence (a) and absence (b) of *in-situ* grown RuO_2.

Table S1. XRD refined parameters of the samples.

Samples	Space group	R_{wp} (%)	R_p (%)	Cell parameter (Å)	Cell volume ($Å^3$)
SCF	Pm-3m	4.416	3.452	a=b=c=3.9373	61.0373
SCFR	Pm-3m	5.046	4.048	a=b=c=3.9478	61.5270

Table S2. Specific areas and pore sizes of the samples

Samples	Specific areas ($m^2\ g^{-1}$)	Pore sizes (nm)
SCF	5.701	3.71
SCFR	18.056	10.05
SCFR-Ru	12.822	2.13
SCFR-RuO_2	11.712	2.00

Table S3. XPS peaks deconvolution results.

Samples	Ce 3d (%)		Fe 3p (%)			O 1s (%)		
	Ce^{3+}	Ce^{4+}	Fe^{2+}	Fe^{3+}	Fe^{4+}	O_{lat}	O_{ads}	O_{H2O}
SCFR	13.33	86.67	16.51	63.76	19.73	39.55	56.19	4.26
SCFR-Ru	28.30	71.70	30.08	56.78	13.14	36.00	62.56	1.44
SCFR-RuO_2	17.07	82.98	24.74	52.23	23.03	42.05	56.82	1.13

Table S4. Comparison of the electrochemical performance of SCFR-H-O with some previously reported catalysts for OER[1-18].

Catalysts	Overpotential at 10 mA cm^{-2} (mV)	Tafel slope (mV dec^{-1})	Catalyst loading (mg cm^{-2})	Ref
SCFR-RuO_2	295	77	0.204	This work
Pt/C	465	NA	0.209	1
IrO_2	340	53.8	0.209	2
RuO_2/C	390	NA	0.14	3
$Sr_xCo_{0.8}Fe_{0.2}O_3$	400	49	0.3	4
$SrCo_{0.8}Fe_{0.5-x}O_{3-\delta}/Fe_xO_y$	352	79	0.243	5
$SrCo_{0.8}Fe_{0.2}O_3$	530	NA	0.232	6
$Sr_2Fe_2O_{6-\delta}$	480	60	NA	7
$SrFeO_3$	500	75	0.232	8
$CaFeO_3$	520	82	0.022	9
$BaFeO_3$	493	NA	NA	10
$LaFeO_3$	466	90	0.407	11
3DOM-$LaFeO_3$	420	62	0.232	12
$La_{1-x}Sr_xCo_{1-y}Fe_yO_{3-\delta}$	440	109	0.2	13
$La_{1.5}Sr_{0.5}NiMn_{0.5}Ru_{0.5}O_6$	430	NA	0.05	14
$Ba_{0.5}Sr_{0.5}Co_{0.8}Fe_{0.2}O_{3-\delta}$	500	65	0.232	15
$La_{0.2}Sr_{0.8}FeO_{3-\delta}$	370	60	0.232	8
$SrFe_{0.9}Ti_{0.1}O_3$	520	102	0.32	16
80nm $LaCoO_3$	490	69	0.25	17
Bulk $LaFe_{0.8}Co_{0.2}O_3$	460	70	0.232	12
$SrNb_{0.1}Co_{0.7}Fe_{0.2}O_{3-\delta}$	500	76	0.232	6
$PrBa_{0.5}Sr_{0.5}Co_{1.5}Fe_{0.5}O_{5+\delta}$	358	52	0.202	18

References

1. N. -I. Kim, Y. J. Sa, T. S. Yoo, S. R. Choi, R. A. Afzal, T. Choi, Y. -S. Seo, K. -S. Lee, J. Y. Hwang, W. S. Choi, S. H. Joo, J. -Y. Park, *Sci. Adv.*, 2018, **4**, eaap9360.
2. R. Zhang, Y.-C. Zhang, L. Pan, G.-Q. Shen, N. Mahmood, Y.-H. Ma, Y. Shi, W. Jia, L. Wang, X. Zhang, W. Xu and J.-J. Zou, *Acs. Catal.*, 2018, **8**, 3803-3811.
3. Y. Zhan, C. Xu, M. Lu, Z. Liu and J. Y. Lee, *J. Mater. Chem. A*, 2014, **2**, 16217-16223.
4. Y. Da, L. Zeng, C. Wang, C. Gong and L. Cui, *Electrochim. Acta*, 2019, **300**, 85-92.
5. Y. Yi, Q. Wu, J. Li, W. Yao and C. Cui, *ACS Appl. Mater. Interfaces*, 2021, **13**, 17439-17449.
6. Y. Zhu, W. Zhou, Z. G. Chen, Y. Chen, C. Su, M. O. Tade and Z. Shao, *Angew. Chem. Int. Ed. Engl.*, 2015, **54**, 3897-3901.
7. R. K. Hona and F. Ramezanipour, *Angew. Chem. Int. Ed. Engl.*, 2019, **58**, 2060-2063.
8. S. She, J. Yu, W. Tang, Y. Zhu, Y. Chen, J. Sunarso, W. Zhou and Z. Shao, *ACS Appl. Mater. Interfaces*, 2018, **10**, 11715-11721.
9. R. Sankannavar and A. Sarkar, *Int. J. Hydrogen Energy*, 2018, **43**, 4682-4690.
10. K. Zhu, H. Liu, X. Li, Q. Li, J. Wang, X. Zhu and W. Yang, *Electrochim. Acta*, 2017, **241**, 433-439.
11. H. Wang, J. Wang, Y. Pi, Q. Shao, Y. Tan and X. Huang, *Angew. Chem. Int. Ed. Engl.*, 2019, **58**, 2316-2320.
12. J. Dai, Y. Zhu, Y. Zhong, J. Miao, B. Lin, W. Zhou and Z. Shao, *Adv. Mater. Interfaces*, 2018, **6**, 1801317.
13. R. Majee, S. Chakraborty, H. G. Salunke and S. Bhattacharyya, *ACS Appl. Energy Mater.*, 2018, **1**, 3342-3350.
14. M. Retuerto, F. Calle-Vallejo, L. Pascual, G. Lumbeeck, M. T. Fernandez-Diaz, M. Croft, J. Gopalakrishnan, M. A. Pena, J. Hadermann, M. Greenblatt and S. Rojas, *ACS Appl. Mater. Interfaces*, 2019, **11**, 21454-21464.
15. W. Z. Gao Chen, Daqin Guan, Jaka Sunarso, Yanping Zhu, Xuefeng Hu, Wei Zhang, Zongping Shao, *Sci. Adv.*, 2017, **3**, e1603206.
16. C. Su, W. Wang, Y. Chen, G. Yang, X. Xu, M. O. Tade and Z. Shao, *ACS Appl. Mater. Interfaces*, 2015, **7**, 17663-17670.
17. S. Zhou, X. Miao, X. Zhao, C. Ma, Y. Qiu, Z. Hu, J. Zhao, L. Shi and J. Zeng, *Nat. Commun.*, 2016, **7**, 11510.
18. B. Zhao, L. Zhang, D. Zhen, S. Yoo, Y. Ding, D. Chen, Y. Chen, Q. Zhang, B. Doyle, X. Xiong and M. Liu, *Nat. Commun.*, 2017, **8**, 14586.